On the analysis of rapidly sampled fMRI data

Jingyuan E. Chen[a,b,c*], Jonathan R. Polimeni[b,c,d], Saskia Bollmann[e], Gary H. Glover[a]
[a] Department of Radiology, Stanford University, Stanford, CA, USA
[b] Athinoula A. Martinos Center for Biomedical Imaging, Massachusetts General Hospital, Boston, MA, USA
[c] Department of Radiology, Harvard Medical School, Boston, MA, USA
[d] Harvard-Massachusetts Institute of Technology Division of Health Sciences and Technology, Cambridge, MA, USA
[e] Centre for Advanced Imaging, The University of Queensland, Brisbane QLD 4072, Australia

Supplementary material

SM1. Experimental Data

Data were collected with two 3T scanners, referred hereafter as Sc1 and Sc2.

Sc1: GE Premier (Milwaukee, WI) with a vender-supplied 48-channel radio frequency (RF) coil.

Sc2: GE Signa Discovery 750 (Milwaukee, WI) with a vender-supplied 8-channel RF coil or a 32-channel RF coil (NOVA Medical, Wilmington, MA).

A simultaneous multi-slice (SMS) echo planar imaging (EPI) with blipped controlled aliasing in parallel imaging (CAIPI) sequence (Setsompop et al., 2012) was used for accelerated T_2^*-weighted functional imaging. For all scan sessions, respiration and cardiac data were measured using the vender-supplied pneumatic respiratory belt placed on the upper abdomen, pulse oximetry photoplethysmograph placed on a finger and recorded with the scanner's built-in physiological monitoring system, sampling at 25 Hz and 100 Hz rates for respiratory and cardiac waveforms, respectively.

All subjects provided informed consent in accordance with the Stanford Institutional Review Board.

• S1A

Acquisition. This single subject data was collected with Sc1, SMS acceleration factor = 3, 15 axial slices, voxel size 1.72×1.72×3 mm^3, FOV = 22 cm, TE = 30 ms.

Two 6-min block-design visual task scans were acquired (flashing checkerboard stimuli, 12 blocks per scan, 15/15 s on/off). Scan1: TR = 350 ms, flip angle = 40°; scan2: TR = 2000 ms, flip angle = 77°.

Analysis. The first 6 s of each scan were discarded to allow the MR signal to achieve T_1 equilibration. Basic preprocessing steps included slice timing correction, removal of linear and quadratic scanner drifts, and regression of six motion parameters with custom C and MATLAB routines. Quasi-periodic physiological fluctuations and slow physiological processes correlated with respiration per unit time (RVT) and heart rate variability (HRV) were removed using RETROICOR (Glover et al., 2000) and RVHRcor (Chang et al., 2009).

• S1B

TR = 0.35 s

Acquisition. This dataset included 10 healthy subjects (4 females, aged 36±12 years). Data were collected with Sc2 using the 32-channel RF coil, SMS acceleration factor = 6, CAIPI shift of FOV/3, flip angle = 40°, 30 axial slices, voxel size 3.14×3.14×4 mm^3, FOV = 22 cm, TE = 30 ms. Each subject underwent a 10-min resting-state scan and an additional 7-sec scan with reversed phase encoding directions (to correct for susceptibility-induced distortions).

Analysis. After reconstruction, data were corrected for susceptibility-induced distortions using the FSL TOPUP toolbox (http:// fsl.fmrib.ox.ac.uk/fsl/fslwiki/TOPUP). The first 29 frames (10 s) of each scan were discarded to allow the MR signal to achieve T_1 equilibration. Basic preprocessing steps included slice timing correction, removal of linear and quadratic scanner drifts, and regression of six motion parameters with custom C and MATLAB routines. Quasi-periodical physiological fluctuations and slow physiological processes correlated with RVT and HRV were removed using RETROICOR and RVHRcor. Amplitude spectra of the global signal (averaged across time series within the gray matter mask, then normalized to z-score) were calculated for each subject, then averaged across subjects (Fig. 2 (b), TR = 0.35 s, black curve).

TR = 2 s

Acquisition. This dataset included 21 healthy subjects (10 females, aged 31±10 years). Data were collected with Sc2 using the 8-channel RF coil. A gradient echo spiral-in/out pulse sequence (Glover and Law, 2001) was used for T_2^*-weighted functional imaging (TR/TE = 2000/30 ms, flip angle = 77°, FOV = 22 cm, 31 oblique axial slices, voxel size 3.43×3.43×4 mm^3, 1 mm slice skip). Each subject underwent an 8-min resting state scan. Subjects' motions were minimized with a bite bar (the average of root-mean-square translations within a scan for all scans was less than 70 µm).

Analysis. The first 10 frames (20 s) of each scan were discarded to allow the MR signal to achieve T_1 equilibration. Basic preprocessing steps included slice timing correction, removal of linear and quadratic scanner drifts, and regression of six motion parameters with custom C and MATLAB routines. Quasi-periodic physiological fluctuations and slow physiological processes correlated with RVT and HRV were removed using RETROICOR and RVHRcor. Datasets were further spatially smoothed using a 3D Gaussian kernel (FWHM = 4 mm). Amplitude spectra of the global signal (averaged across time series within the gray matter mask, then normalized to z-score) were calculated for each subject, then averaged across subjects (Fig. 2 (b), TR = 2 s, black curve).

- **S1C**

Acquisition. This single subject data was collected with Sc2, SMS acceleration factor = 6, CAIPI shift of FOV/3, 30 axial slices, voxel size 3.43×3.43×4 mm^3, FOV = 22 cm, TE = 30 ms. This subject underwent two visual + auditory task scans (7 blocks per scan, 15/15 s on/off). Scan1: TR = 400 ms, flip angle = 42°; scan2: TR = 2000 ms, flip angle = 77°.

Analysis. The first 10 s of each scan were discarded to allow the MR signal to achieve T1 equilibration. Basic preprocessing steps included slice timing correction and motion correction. Nuisance factors (linear and quadratic scanner drifts, six motion parameters, quasi-periodical physiological fluctuations and slow RVT/HRV regressors) were included along with the ideal task response and the associated temporal derivative in the GLM-based task analysis. Instead of the 'pre-whitening' approach, t-scores were calculated according to (Worsley and Friston, 1995). Ordinary least square fittings were first applied to estimate the fitting parameters associated with different task regressors. DOFs of t distributions were then adjusted according to the serial correlations of the fitted residuals. These analyses were implemented using custom matlab and R routines.

- **S1D**

Acquisition. This single subject data was collected with Sc1, SMS acceleration factor = 3, 15 axial slices, image resolution 2.3×2.3×3 mm^3, resampled to voxel size 1.72×1.72×3 mm^3, FOV = 22 cm, TE = 30 ms.

This subject underwent four 6-min block-design visual-task scans (flashing checkerboard stimuli, 12 blocks per scan, 15/15 s on/off). TR = 400/800/1400/2000 ms, flip angle = 42°/56°/69°/77° for four separate scans.

Preprocessing. The first 6 s of each scan were discarded to allow the MR signal to achieve T1 equilibration. Basic preprocessing steps included slice timing correction and motion correction.

GLM-based task activation (Fig. 4 (a, b)). Nuisance factors (linear and quadratic scanner drifts, six motion parameters, quasi-periodical physiological fluctuations and slow RVT/HRV regressors) were included along with the ideal task response and the associated temporal derivative in the GLM-based task analysis. T-scores were derived using AFNI's 3dREMLfit. The t-score map averaged across four functional scans was thresholded ($t > 8$) to generate an overall voxel mask. T-scores of voxels within the mask were averaged for each functional scan.

Linear Pearson correlation analysis (Fig. 4 (c, d)). Nuisance factors (linear and quadratic scanner drifts, six motion parameters, quasi-periodical physiological fluctuations and slow RVT/HRV regressors) were first linearly projected out from each voxel's time series. MELODIC ICA (https://fsl.fmrib.ox.ac.uk/fsl/fslwiki/MELODIC) was performed on the cleaned time series to identify the seed region of interest (ROI) in the auditory cortex (the region with peak z-scores, ROI size = 49 voxels). The serial correlation of each voxel was quantified using an ARMA (1,1) model. Linear Pearson correlation coefficients and the associated t-scores were computed using custom MATLAB and R routines. The t-score map averaged across four functional scans (‘Raw’, without pre-whitening or low-pass filtering) was thresholded ($t > 5$, the contralateral side of the seed ROI) to generate an overall voxel mask. T-scores of voxels within the mask were averaged for each functional scan.

SM2. Respiratory artifacts in motion estimates

(1) Aliased respiratory artifacts in motion estimates (at long TRs)

To offer an example on how the respiratory effects (discussed in section 3.1 of the main text) may manifest in long-TR acquisitions, rotational motion estimates and the respiratory waveform of HCP subject 02 (Fig. 1 (a)) were down-sampled at different TR values. At long TR values (e.g., TR = 3.6 s), respiratory effects (section 3.1) in the motion estimates can alias into low frequencies (< 0.1 Hz) that overlap with the spectra of neural activity, and therefore become less noticeable.

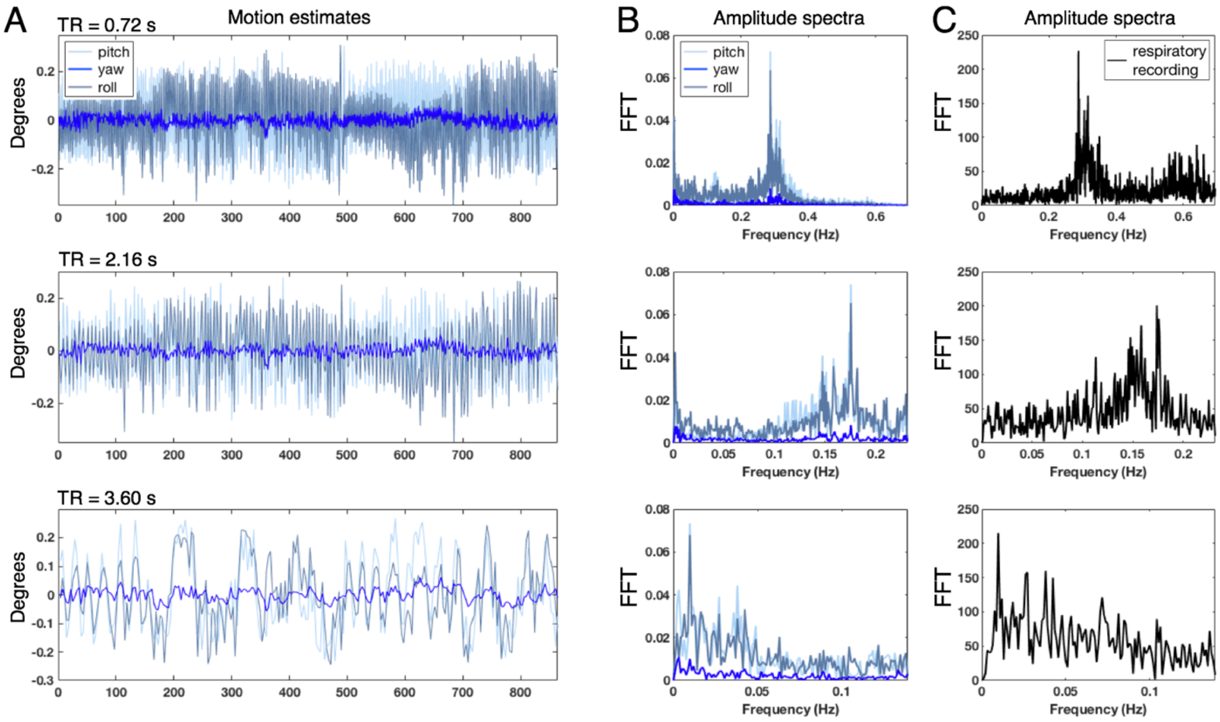

Supplementary Figure 1 (A) rotational motion estimates down-sampled at different TR values; (B) amplitude spectra of the down-sampled motion estimates; (C) amplitude spectra of the down-sampled physiological recordings.

SM 2 (2) Illustration of respiratory artifacts in motion estimates caused by different mechanisms

Motion estimates are shown for one subject under two scan conditions in which either respiratory-induced field perturbations or head movements predominated: (1) field perturbations: the subject performed paced breathing (inhale/exhale 3/3 s) following instructions displayed on the screen, while keeping the head still; (2) mechanical movements: the subject held her breath and voluntarily nodded her head every a few seconds (self-paced). Two EPI acquisitions with different phase encoding (PE) directions were collected for both conditions: acquisition 1 (TR/TE = 1500/30 ms, PE: Anterior-Posterior); acquisition 2 (TR/TE = 1730/35 ms, PE: Left-Right). This experiment was performed in 3T (Siemens Prisma scanner), voxel size 2.5×2.5×1.5 mm^3, FOV = 200 mm.

Motion estimates of these EPI scans are shown in supplementary figure 2: as noted by Fair et al., (2018), respiratory artifacts caused by field perturbations are prominent along PE directions, and observable in other directions as well due to cross-talk effects; respiratory artifacts caused by mechanical head movements (which exhibit no differences between different PE directions) dominate in ‘pitch’ measure, as the subject voluntarily nodded her head.

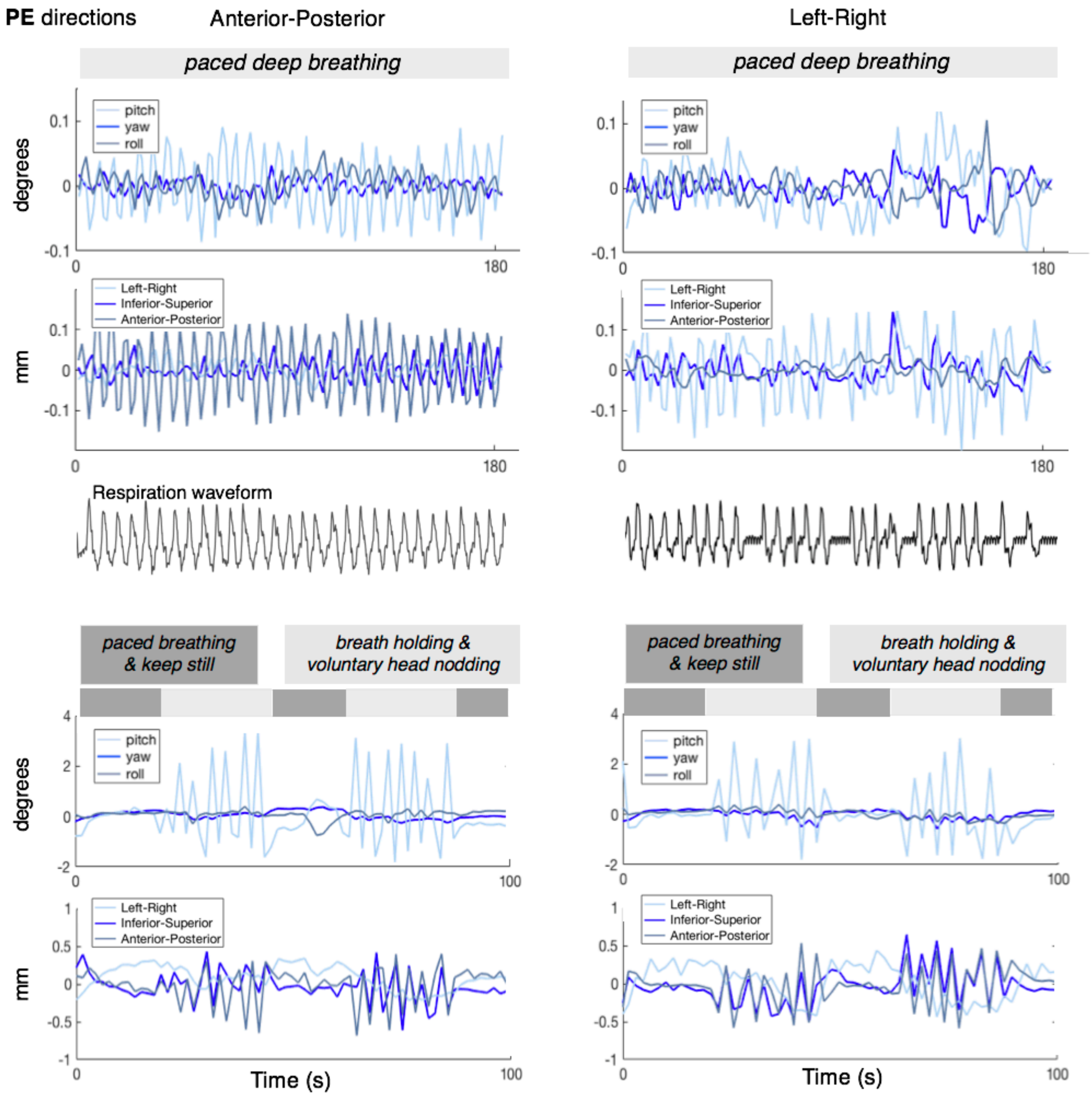

Supplementary Figure 2 Motion estimates in two scan conditions under which different mechanisms of artifacts dominate: (1) paced deep breathing (field perturbation), and (2) breath holding & voluntary head nodding (mechanical movements).

SM3. Replication of Fig. 4 in a second subject

Task design, data acquisition and analysis procedure followed supplementary material S1D. As the T-scores for both task activation and functional connectivity were lower in the 2nd subject compared to 1st subject (results shown in Fig. 4), lower T-score thresholds were used to select the overall voxel mask: ($t > 6$ for GLM-based task activation; and $t > 4$ for Linear Pearson correlation analysis).

Supplementary Figure 3 (a) GLM-based single-subject visual task activation at different TR values without ('Raw') and with spatial smoothing. (b) (Left) Predicted ($\mathrm{tSNR} \times \sqrt{N}$, N is the number of temporal frames) and (Right) estimated (real data) t-score gains (i.e., divided by the t-score values at TR = 2 s) for the data shown in panel (a). Data were smoothed by different spatial extents with isotropic Gaussian kernels at different FWHMs (highlighted with distinct colors) to manipulate the fractional contribution of physiological and white noise in the real data. (c) Linear Pearson correlation based auditory network patterns at different TRs and preprocessing. (d) Predicted ($\mathrm{tSNR} \times \sqrt{N}$) and estimated (real data) t-score gains in (c). Note that only the contralateral side of the seed (highlighted by a red rectangle in (c)) was included for comparison. The statistical gains of different preprocessing steps were normalized by the t-scores at TR = 2 s of the 'Raw' data. See supplementary material S1D for descriptions of task design, data acquisition and analysis.

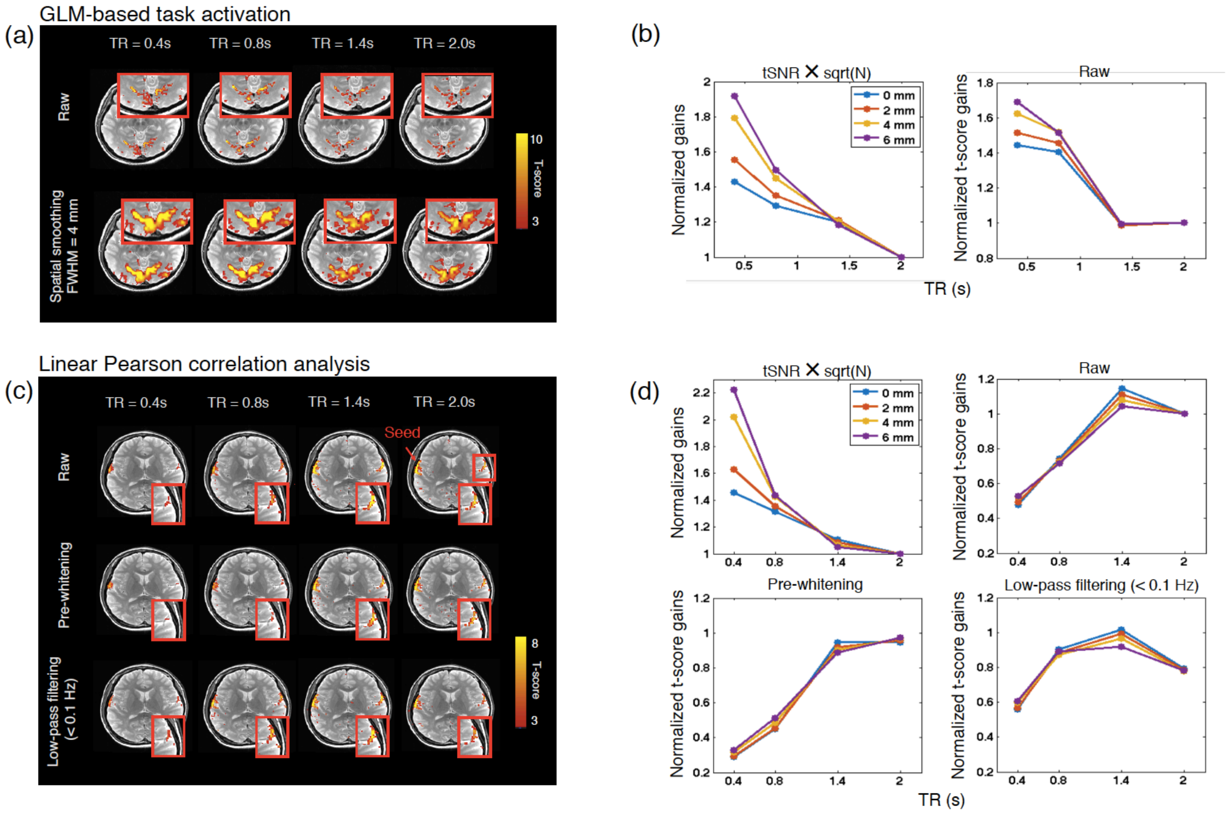

SM4. Simulations of tSNR biases in multiple-channel coil arrays, when considering the statistics of image magnitudes as Rician or non-central chi distributions

• tSNR simulated with Gaussian noise (following Appendix A in the main text)

The relationship between $\mathrm{tSNR}_{\mathrm{TR}}$ (tSNR at different TR values) and $\mathrm{SNR}_{0,\mathrm{TR}}$ (image SNR at different TR values) can be defined as:

$$\mathrm{tSNR}_{\mathrm{TR}} = \frac{S_{\mathrm{TR}}}{\sqrt{\mathrm{Var}(N_{\mathrm{p,TR}})+\mathrm{Var}(N_{\mathrm{w,TR}})}} = \frac{S_{\mathrm{TR}}}{k_{\mathrm{TR}}\sqrt{\mathrm{Var}(N_{\mathrm{w,TR}})}} = \frac{1}{k_{\mathrm{TR}}}\cdot \mathrm{SNR}_{0,\mathrm{TR}},$$

where

$$\mathrm{SNR}_{0,\mathrm{TR}} = \frac{A_{\mathrm{TR}}}{A_2}\cdot \mathrm{SNR}_{0,2},$$

and

$$k_{\mathrm{TR}} = \sqrt{\frac{\mathrm{Var}(N_{\mathrm{p,TR}})}{\mathrm{Var}(N_{\mathrm{w,TR}})}+1} = \sqrt{\frac{1}{1-\varphi_{\mathrm{TR}}^2}\cdot\frac{\sigma_{\mathrm{p,TR}}^2}{\sigma_{\mathrm{w,TR}}^2}+1}.$$

S_{TR}, $N_{\mathrm{p,TR}}$ and $N_{\mathrm{w,TR}}$ refer to the signal, physiological and white noise at different TR values (see Appendix A in the main text for statistical characteristics of $N_{\mathrm{p,TR}}$ and $N_{\mathrm{w,TR}}$, and the definition of the Ernst angle scaling factor A_{TR}).

• tSNR simulated with noise following a non-central chi distribution

For simplicity, we assume i.i.d. noise within each coil channels as well as independent noise with equal variance across channels (i.e., the channel noise covariance matrix is assumed to be the identity matrix). The image magnitude distributions can therefore be simulated using non-central chi distributions, which are generalizations of the Rician noise model for magnitude-valued data to multi-channel array coil data, detailed in eqn. [1] by Constantinides et al. (1997).

• Bias in measured tSNR and statistical gains

Simulated results of “true” tSNR (modeled with Gaussian-distributed noise) and “apparent” tSNR (modeled with non-central-chi-distributed noise) under different $\mathrm{SNR}_{0,2}$ conditions are shown in supplementary Figure 4 below. The “true” tSNR is by definition the same for each channel count, and therefore consistent across panels. In the 1 channel case, the non-central chi noise model reduces to a Rician noise model: the “apparent” tSNR remains non-zero even at very low “true” tSNR levels, and the discrepancy between “true” tSNRs and “apparent” tSNRs increases with the number of channels. As SNR increases, the “apparent” tSNR will gradually converge to the “true” tSNR in the 1 channel simulations, which is expected as Rician noise model approximates a standard Gaussian distribution at high signal levels.

Consequently, simulated statistical gains using “apparent” tSNR deviate from “true” tSNR at low SNR and large coil arrays, advising caution in invoking Gaussian noise models under these conditions.

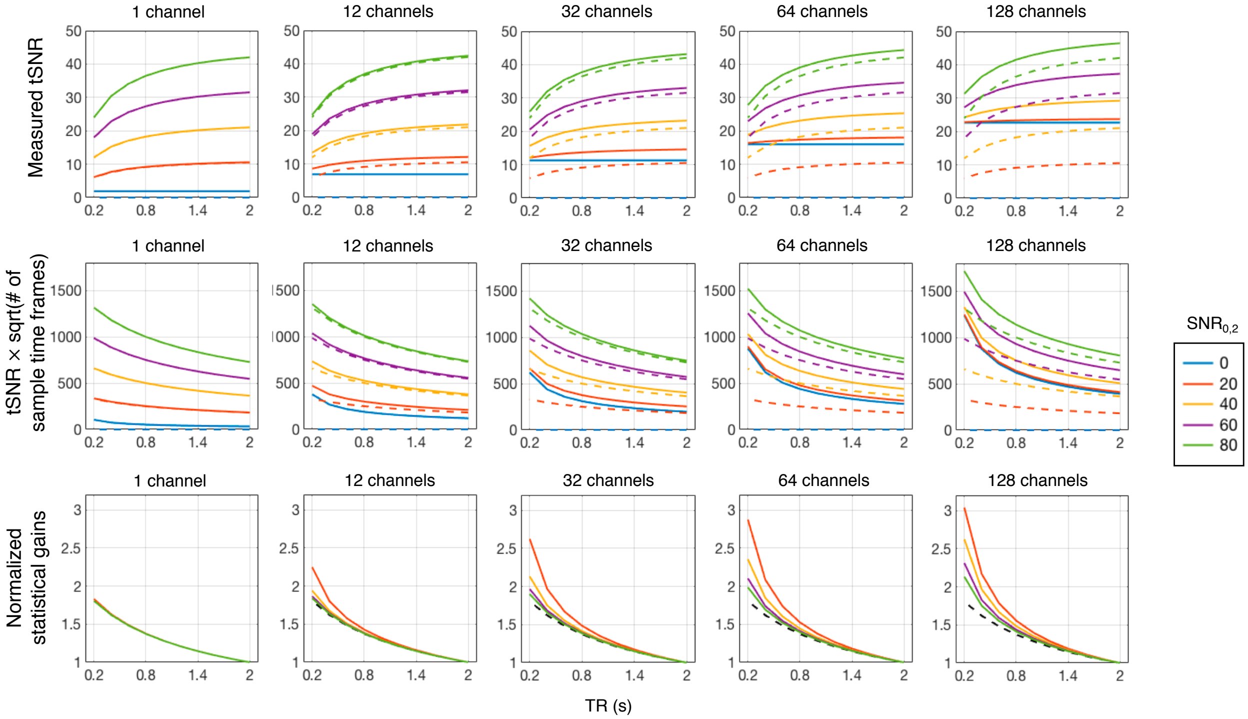

Supplementary Figure 4 Magnitude detection biases the tSNR calculation and statistical gains increasingly at low $\mathrm{SNR}_{0,2}$ and larger coil arrays. “true” tSNR (dashed lines) was modeled with Gaussian-distributed noise, and “apparent” tSNR (solid lines) was modeled with non-central-chi-distributed noise. Results under different $\mathrm{SNR}_{0,2}$ conditions (assuming physiological and white noise parameters: $\varphi_{0.35} = 0.9089$, $\sigma^2_{p,0.35} = 0.1221$, and $\sigma^2_{w,0.35} = 1.3069$; tissue $\mathrm{T}_1 = 1350\ \mathrm{ms}$ at 3T) are shown in distinct colors. Statistical results (approximated by $tSNR \times$ sqrt (# of sample time frames in a 10-min long scan)) and normalized statistical gains (relative to TR = 2 s, the true statistical gain was colored in black as it is invariant across different $\mathrm{SNR}_{0,2}$ values) were shown in the middle and bottom rows.

SM5. Derivation of eqn. (A.4 A.5)

If the physiological noise at $\mathrm{TR} = \Delta t$, i.e., $\{N_{p,\Delta t}[n]\}$, is down-sampled by an integer factor *K*, the resulting process $\{N_{p,K\Delta t}[n]\}$ is still an AR-1 process:

$$N_{p,K\Delta t}[n] = N_{p,\Delta t}[K\cdot n] = \varphi_{\Delta t}^{K}\cdot N_{p,\Delta t}[K\cdot(n-1)] + \varepsilon_{p,\Delta t}[K\cdot n] + \varphi_{\Delta t}\cdot\varepsilon_{p,\Delta t}[K\cdot n-1] + \varphi_{\Delta t}^{2}\cdot\varepsilon_{p,\Delta t}[K\cdot n-2] + \cdots\ \varphi_{\Delta t}^{K-1}\cdot\varepsilon_{p,\Delta t}[K\cdot n-K+1] = \varphi_{K\Delta t}\cdot N_{p,K\Delta t}[n-1] + \varepsilon_{p,K\Delta t}[n],$$

with

$$\varphi_{K\Delta t} = \varphi_{\Delta t}^{K}$$

and

$$\varepsilon_{p,K\Delta t}[n] = \varepsilon_{p,\Delta t}[K\cdot n] + \varphi_{\Delta t}\cdot\varepsilon_{p,\Delta t}[K\cdot n-1] + \varphi_{\Delta t}^{2}\cdot\varepsilon_{p,\Delta t}[K\cdot n-2] + \cdots\ \varphi_{\Delta t}^{K-1}\varepsilon_{p,\Delta t}[K\cdot n-K+1].$$

Given that $\varepsilon_{p,\Delta t}[n]$ is a white noise process with zero mean and constant variance $\sigma_{p,\Delta t}^{2}$, we have:

$$\sigma_{p,K\Delta t}^{2} = \left(1+\varphi_{\Delta t}^{2}+\varphi_{\Delta t}^{4}\ \ldots\ \varphi_{\Delta t}^{2(K-1)}\right)\cdot\sigma_{p,\Delta t}^{2} = \frac{1-\varphi_{\Delta t}^{2K}}{1-\varphi_{\Delta t}^{2}}\sigma_{p,\Delta t}^{2} = \frac{1-\varphi_{K\Delta t}^{2}}{1-\varphi_{\Delta t}^{2}}\sigma_{p,\Delta t}^{2}.$$

We further let Δt be sufficiently small such that any TR value is divisible by Δt, the model parameters at different TRs follow:

$$\frac{\log\left(\varphi_{\mathrm{TR}}\right)}{\left[\frac{TR}{\Delta t}\right]} = \log\left(\varphi_{\Delta t}\right)$$

and

$$\frac{\sigma_{\mathrm{TR}}^{2}}{1-\varphi_{\mathrm{TR}}^{2}} = \frac{\sigma_{p,\Delta t}^{2}}{1-\varphi_{\Delta t}^{2}}.$$

We can further derive the relationship between $\varphi_{\mathrm{TR}}, \sigma_{\mathrm{TR}}^{2}$ and $\varphi_{0.35}, \sigma_{0.35}^{2}$ as:

$$\varphi_{\mathrm{TR}} = e^{\log(\varphi_{0.35})\cdot\mathrm{TR}/0.35},$$
$$\sigma_{p,\mathrm{TR}}^{2} = \frac{1-\varphi_{\mathrm{TR}}^{2}}{1-\varphi_{0.35}^{2}}\cdot\sigma_{p,0.35}^{2}.$$

After adjusting the noise amplitudes according to Ernst angles, we obtain the expression in eqn. (A4, A5).

References

Chang, C., Cunningham, J.P., Glover, G.H., 2009. Influence of heart rate on the BOLD signal: the cardiac response function. Neuroimage 44, 857-869.

Constantinides, C.D., Atalar, E., McVeigh, E.R., 1997. Signal-to-noise measurements in magnitude images from NMR phased arrays. Magn Reson Med 38, 852-857.

Glover, G.H., Law, C.S., 2001. Spiral-in/out BOLD fMRI for increased SNR and reduced susceptibility artifacts. Magn Reson Med 46, 515-522.

Glover, G.H., Li, T.Q., Ress, D., 2000. Image-based method for retrospective correction of physiological motion effects in fMRI: RETROICOR. Magn Reson Med 44, 162-167.

Setsompop, K., Gagoski, B.A., Polimeni, J.R., Witzel, T., Wedeen, V.J., Wald, L.L., 2012. Blipped-controlled aliasing in parallel imaging for simultaneous multislice echo planar imaging with reduced g-factor penalty. Magn Reson Med 67, 1210-1224.

Worsley, K.J., Friston, K.J., 1995. Analysis of fMRI time-series revisited--again. Neuroimage 2, 173-181.